



# 3D High Resolution Imaging of Human Heart for Visualization of the Cardiac Structure

Kylian Haliot<sup>1,2,3</sup>✉, Julie Magat<sup>1,2,3</sup>, Valéry Ozenne<sup>1,2,3</sup>,  
Emma Abell<sup>1,2,3</sup>, Virginie Dubes<sup>1,2,3</sup>, Laura Bear<sup>1,2,3</sup>,  
Stephen H. Gilbert<sup>4</sup>, Mark L. Trew<sup>5</sup>, Michel Haissaguerre<sup>1,2,6</sup>,  
Bruno Quesson<sup>1,2,3</sup>, and Olivier Bernus<sup>1,2,3</sup>

<sup>1</sup> IHU Liryc, Electrophysiology and Heart Modeling Institute,  
Foundation Bordeaux Université, 33600 Pessac-Bordeaux, France  
kylian.haliot@ihu-liryc.fr

<sup>2</sup> Univ. Bordeaux, Centre de recherche Cardio-Thoracique de Bordeaux, U1045,  
33000 Bordeaux, France

<sup>3</sup> INSERM, Centre de recherche Cardio-Thoracique de Bordeaux, U1045,  
33000 Bordeaux, France

<sup>4</sup> Mathematical Cell Physiology, Max Delbrück Centre for Molecular Medicine  
in the Helmholtz Association, 13125 Berlin-Buch, Germany

<sup>5</sup> Bioengineering Institute, Department of Physiology, University of Auckland,  
Auckland, New Zealand

<sup>6</sup> Bordeaux University Hospital (CHU), Electrophysiology and Ablation Unit,  
33600 Pessac, France

**Abstract.** Imaging of cardiac structure is thus essential for understanding both electrical propagation and efficient contraction in human models. The processing pipeline of diffusion tensor imaging (DTI) and structure tensor imaging (STI) is described and the first *ex vivo* demonstration of this approach in a human heart is provided at 9.4T.

A human heart was fixed in formaldehyde with gadolinium then immersed in Fomblin. MRI acquisitions were performed at 9.4T/30 cm with a 7 elements transmit/receive coil. 3D spin-echo DTI at  $600 \times 600 \times 600 \mu\text{m}^3$  and 3D FLASH echo image at  $150 \times 150 \times 150 \mu\text{m}^3$  were produced. Tensor extraction and analysis were performed on both volumes.

3D gradient echo at  $150 \times 150 \times 150 \mu\text{m}^3$  allows direct visualization of detailed structure of LV. Abrupt change in sheetlet orientation is observed in the LV and is confirmed with STI. The DTI helix angle has a smooth transmural change from endocardium to epicardium. Both the helix and transverse angles are shown to be similar between DTI and STI. The sheetlet organization between both acquisitions displays the same pattern even though local angle differences are demonstrated.

In conclusion, these preliminary results are promising for investigating 3D structural characterization of normal/pathologic cardiac organization in human. It opens new perspectives to better understand the links between structural remodeling and electrical disorders of the heart.

**Keywords:** Cardiac microstructure · Sheetlet organization · High field MRI · Helix angles · Structure tensor · Diffusion tensor

## 1 Introduction

Efficient contraction and electrical propagation are key parameters in the normal function of the heart, and they are influenced by the myocardial structure [1]. Visualizing and quantifying myocardial arrangement is important for assessing impact on cardiac function.

Two cardiac organizations have been described [2, 3]:

- The myocyte orientation defined by the long axis of the myocytes, shows a regular low order organization in the ventricular wall often described as a helical transmural arrangement [4].
- The orientation of the myolaminae, i.e. the laminar architecture, is more complex, and comprises sheetlets disconnected by collagenous bundle interstices [5].

Both these architectures help defining an orthotropic myocardial basis along three orthogonal directions: normal to the sheetlet plane, normal to the fiber axis in the sheetlet plane and collinear to the fiber axis.

Magnetic Resonance Imaging (MRI) technique can provide information on the myocardial myocyte orientation and the myolaminar structure covering the whole heart. Diffusion Tensor Imaging (DTI) has been applied to investigate cardiac myocyte orientation *in vivo* [6, 7] and *ex vivo* in 3D on several species [7–11] including human [3]. DTI was also validated by comparison to histology [12]. Following from this earlier work, 3D high resolution MRI (HR-MRI) acquisition with at  $50 \times 50 \times 50 \mu\text{m}^3$  isotropic resolution was proposed and validated by Gilbert et al. [13] to visualize and quantify cardiac microstructure in rats. They demonstrated that sheetlet orientation found using structure tensor imaging (STI) was proved superior to DTI [14]. However, thus far, this technique on human has been unexplored.

In this study, we apply these approaches to whole *ex vivo* human hearts from patients not eligible to cardiac transplantation. 3D FLASH/ST and diffusion images were acquired at a high spatial resolution using a 9.4T/30 cm magnet and a dedicated transmit/receive MR coil designed for this application. Quantitative structural information are computed from the resulting images using structure tensor analysis and leading to the STI pipeline. The fiber and the sheetlet orientations are extracted from both DTI and STI. The first results on fiber and sheetlet orientations in an intact human heart using a combination of DTI and STI are reported.

## 2 Materials and Methods

### 2.1 Sample Preparation

The heart was obtained through the human donor research project approved by the French Biomedicine Agency. A healthy heart (74 y.o. woman) of dimension  $11 \times 10 \times 12 \text{ cm}^3$  (Fig. 1) was fixed for at least 2 h with formalin containing 2 ml Dotarem (Gadoterate Meglumine, Guerbet, France). Imaging was carried out with the heart removed from formalin and immersed in Fomblin (Solvay Solexis, Inc) oil to reduce susceptibility artifacts at the interface with the tissue [13].

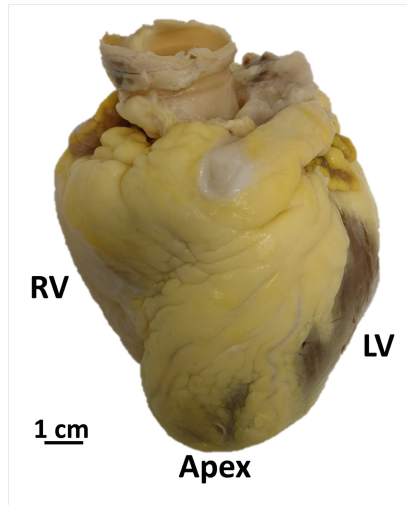


**Fig. 1.** Human donor heart (74 y.o woman) of dimension  $11 \times 10 \times 12 \text{ cm}^3$ . Apex, right ventricle (RV) and left ventricle (LV) are identified. Yellow tissue is corresponding to pericardial fat and brown tissue to cardiac tissue. (Color figure online)

## 2.2 Magnet Set Up

**MRI.** All experiments were performed at 9.4T/30 cm (Bruker Biospin MRI, Ettlingen Germany). A cylindrical (165 mm inner diameter) 7 channels volume array Tx/Rx was used for ex vivo imaging. After acquiring scout images, a standard B1 map using Bloch-Siegert method in 3D (matrix size of  $100 \times 100 \times 32$  and resolution of  $1 \times 1 \times 2 \text{ mm}$ ) was acquired [15].

**3D DTI.** DT-MRI was carried out using a 3D diffusion-weighted spin-echo sequence with TE = 23 ms, TR = 500 ms, at an isotropic resolution of  $600 \times 600 \times 600 \mu\text{m}^3$ . The diffusion gradient had 4.35 ms duration each and with an 11 ms delay between them. Six gradient directions were applied with a b-value of  $1000 \text{ s/mm}^2$ , as described previously [14], and a partial Fourier factor of 1.8 was used, for a total acquisition time of 23 h. Raw diffusion weighted images were processed using Paravison 6.0 to compute the diffusion tensor.

For DTI post processing pipeline in Fig. 2, an N4 bias correction [16] was applied on  $b = 0 \text{ s/mm}^2$  maps to segment the cardiac ventricles, thus avoiding cutting off regions with  $B_1$  inhomogeneity. Binary masks were created using low and high cut-off thresholds based on FA, Trace and diffusion weighted image to remove the background noise. The first DT eigenvector has been shown to correspond to the myocyte orientation [3, 9–11]. The second and third eigenvectors have been associated with the sheetlet in-plane and normal directions respectively,

As described in previous studies [14, 17, 18], all structural information was obtained using a specific cardiac reference system, with an apex-base left ventricle (LV) axis running through the center of the left ventricular cavity. For each voxel in the segmented

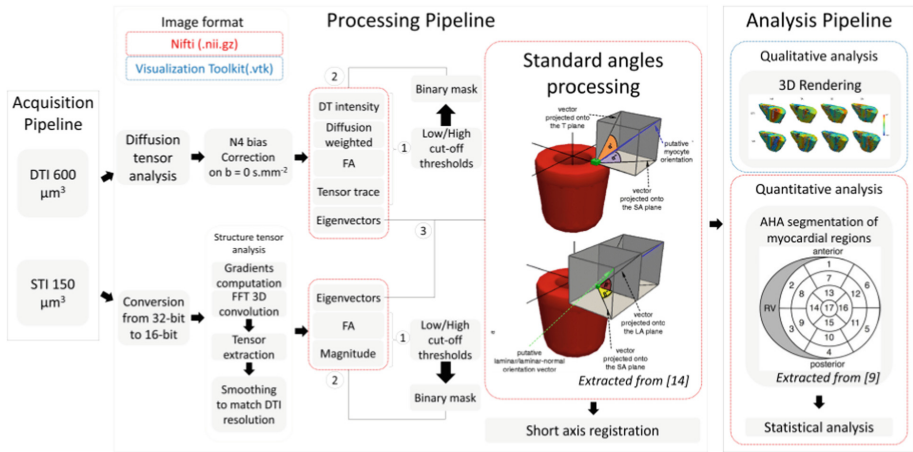


**Fig. 2.** DTI and STI data processing pipeline of the human donor heart of dimension  $11 \times 10 \times 12 \text{ cm}^3$ . Diffusion tensor (DT) spin-echo and structure tensor (ST) gradient-echo data are processed through two different pipelines in the helix angle (HA), transverse angle (TA), sheetlet elevation angle (SE), sheetlet azimuth angle (SA), sheetlet normal elevation angle (NE) and sheetlet normal azimuth angle (NA). The angle maps are then registered in short axis to apply the 17-segment AHA model for quantitative analysis.

datasets, the orientation of myocytes (fibers) and sheetlets were computed in this coordinate system.

**3D STI.** The whole human heart volume was imaged with a 3D FLASH/ST sequence with the following parameters: 12 averages and  $TE = 7 \text{ ms}$ ;  $TR = 30 \text{ ms}$ ; matrix size =  $800 \times 731 \times 665$ ; voxel dimensions =  $150 \mu\text{m}$  isotropic, flip angle =  $32^\circ$ , GRAPPA = 2 in phase encoding direction, for a total acquisition time of 27 h 36 min.

The image-processing pipeline (Fig. 2) was implemented [14] using Matlab 8.6 (The MathWorks Inc., Natick, MA, USA) and VTK libraries: images were converted into a stack of 16-bit images. Then, a structure tensor analysis was carried out: gradients, FFT-based convolution was computed as described in [13, 14] and smoothed at progressive resolution (from  $150 \times 150 \times 150 \mu\text{m}^3$  to  $600 \times 600 \times 600 \mu\text{m}^3$  isotropic ( $800 \times 731 \times 665$  tensors to  $200 \times 183 \times 166$  tensors). Extraction of eigenvalues and eigenvectors was performed. The  $600 \times 600 \times 600 \mu\text{m}^3$  smoothed structure tensor dataset was used to best match the expected diffusion tensor (DT) resolution.

The first eigenvector (largest magnitude eigenvalue) corresponds to the sheetlet/laminae normal direction, the second to the sheetlet/laminae in-plane direction and the third to the myocyte orientation (smallest magnitude eigenvalue) [13, 14].

Binary masks were created using low and high cut-off thresholds based on FA where we chose 0.11 and 1 (meanly between 0.4 and 0.8 in the *ex vivo* heart), Trace and image intensity to remove the background noise.

**Comparison Between STI and DTI.** The first DTI eigenvector was compared to the third STI eigenvector for myocyte orientation and the fiber helix angle (HA) was then computed. The fiber helix angle is the angle between the short axis plane (i.e. the transverse plane) and the projection of the fiber vector onto the wall tangent plane (i.e. the longitudinal plane). The fiber transverse angle (TA) is the angle between the longitudinal plane and the projection of the fiber vector onto the transverse plane as shown on the standard angles processing scheme on Fig. 2.

For sheetlet orientation, the first STI eigenvector was compared to the third DTI eigenvector, which is assumed to be positioned normal to the sheet. The sheetlet elevation angle (SE) is the angle between the short axis plane and the projection of the vector onto the radial plane. The sheetlet azimuth angle (SA) is the angle between the local radial plane and the projection of the vector onto the short axis plane.

**Images Visualization and Quantification.** Image reconstruction was performed using ParaVision 6.0 on a workstation equipped with 512 GB of RAM to process the very large data matrices.

Short axis registration of the parametric volume maps was made using 3D Slicer ([www.slicer.org](http://www.slicer.org)) [19].

3D volume renderings and parametric volume maps were displayed using Paraview (Kitware, Clifton Park, NY) software.

Quantitative transmural maps were sub-divided into regions defined by the 17-segment American Heart Association (AHA) model [20] and post processed using custom written software in Matlab 8.6 (MathWorks Inc., Natic Massachusetts, USA). Descriptive statistics with linear regression ( $R^2$  linearity and slope) and mean curve fitting were performed. A pair wise difference between DTI and STI measurements was performed as described [13]. All quantitative treatments were obtained using GraphPad Prism 8 (GraphPad Software, San Diego, CA) on the segment 7 to 12 of AHA model, corresponding to the mid ventricular region of the heart. Each segment contains a mean of  $19600 \pm 1419.3$  voxels for a total of 117600 voxels in all the considered segments.

## 3 Results

### 3.1 Structural Characterization: A DTI and STI Comparison

**Myocyte Orientation.** Quantitative maps of standard angles describing the myocyte orientation (HA, TA) for both DTI and STI are presented (Fig. 3a–d). Based on DTI eigenvectors, HA map (Fig. 3a) shows a smooth transmural profile myocyte orientation from the LV sub-epicardium ( $-40^\circ$ ) to sub-endocardium ( $90^\circ$ ). In comparison with STI, HA map (Fig. 3b) preserves the same left to right helical orientation (from  $-40^\circ$  to almost  $90^\circ$ ) but with more abrupt transitions. The DTI TA map (Fig. 3c) displays a mean close to  $0^\circ$ , indicating that myocytes orientation stays in the short axis plane. STI TA map (Fig. 3d) is noisier than the DTI, but the overall trend is at values close to  $20^\circ$ .

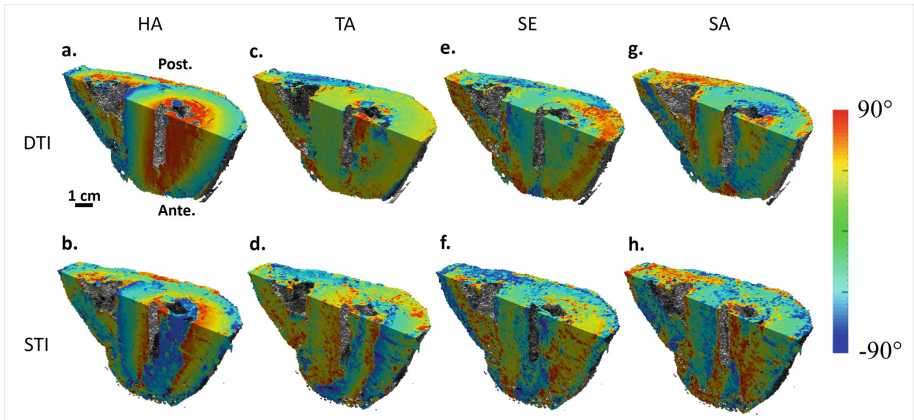


**Fig. 3.** Quantitative angle maps comparison between DTI and STI. Helix angle (HA), transverse angle (TA), sheetlet elevation angle (SE) and sheetlet azimuth angle (SA) in degrees are displayed at  $600 \times 600 \times 600 \mu\text{m}^3$  for both DTI and STI.

Moreover, we observe that both HA and TA maps present an abrupt separation between the LV and RV. The separation between the LV and RV is more pronounced in HA map than in TA map.

Transmural profiles of HA and TA of DTI and STI in the mid ventricular region as measured in segment 7 to 12 based on the AHA heart model (AHA7-12) are presented (Fig. 4a–l). Their linearity and slope are summarized (Table 1) and the pair wise difference between the DTI and STI profiles is presented (Fig. 5a–l). DTI transmural profiles of HA on AHA7-12 (Fig. 4a–f) is found to be mostly linear ( $R^2 \geq 0.8$ ) even though there is a negative slope range of between  $-120.1^\circ$  in the mid anteroseptal region (Fig. 4b, segment 8 on Table 1) to  $-178.3^\circ$  in the mid anterior region (Fig. 4a, segment 7 on Table 1). The pair wise difference of HA (Fig. 5a–f) shows a globally constant variation in the transmural profile with an exception for the segment 7 (Fig. 5a). There is also an offset of about  $10\text{--}20^\circ$  between DT and ST. The pair wise

**Table 1.** Linearity ( $R^2$ ) and coefficient slope of DTI and STI myocyte orientation (helix angle and transverse angle). Linearity and slope were measured from LV endocardium to epicardium.

	DTI Helix angle		STI Helix angle		DTI Transverse angle		STI Transverse angle	
	Linearity	Slope	Linearity	Slope	Linearity	Slope	Linearity	Slope
7	0.80	$-178.3 \pm 1.3$	0.09	$-63.4 \pm 3.0$	0.04	$23.1 \pm 1.5$	0.00	$8.7 \pm 3.2$
8	0.71	$-120.1 \pm 1.0$	0.55	$-136.2 \pm 1.7$	0.25	$38.4 \pm 0.9$	0.34	$111.7 \pm 2.1$
9	0.77	$-126.5 \pm 1.0$	0.56	$-139.9 \pm 1.9$	0.23	$44.6 \pm 1.2$	0.21	$97.2 \pm 2.7$
10	0.62	$-148.5 \pm 1.7$	0.37	$-112.8 \pm 2.1$	0.00	$5.7 \pm 1.8$	0.02	$-31.0 \pm 2.9$
11	0.90	$-153.1 \pm 0.7$	0.77	$-150.3 \pm 1.1$	0.01	$-4.8 \pm 0.7$	0.26	$-61.5 \pm 1.4$
12	0.79	$-153.9 \pm 1.2$	0.52	$-149.6 \pm 2.0$	0.00	$-1.3 \pm 1.0$	0.00	$-4.7 \pm 1.9$

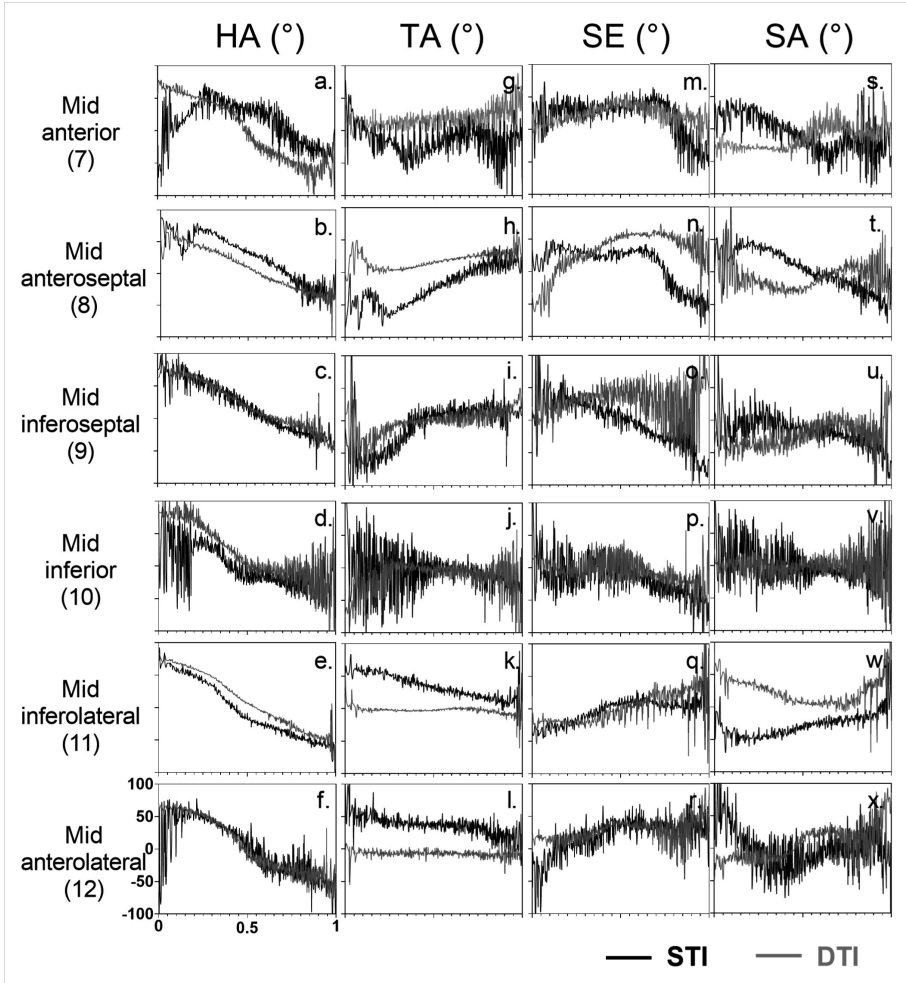


**Fig. 4.** Transmural variation in myocytes and sheetlet orientations comparison between DTI and STI. The 17-segment AHA model defines regions and AHA7-12 of STI (black line) and DTI (gray line) helix angle (HA), transverse angle (TA), sheet elevation (SE) and sheet azimuth (SA) are displayed. Means of angles normalized to wall thickness are given.

difference of TA (Fig. 5g–l) shows a less consistent variation between STI and DTI for segment 8 and 11 (Fig. 5i and k) which goes from 80° in the sub-endocardium to 10° in the sub-epicardium.

Angles profiles of TA (Fig. 4g–l) have a low or absent linearity ( $R^2 \leq 0.25$ ) with a low slope (mean of 17.7° for DTI) and indicates that the orientation is in the short axis plane. STI transmural profiles of HA (Fig. 4a–f) are weakly linear ( $0.55 \leq R^2 \leq 0.8$ ), which represent a higher discrepancy on 3D volume (Fig. 3d), and the slope range is of between  $-150.3^\circ$  in the mid inferolateral (Fig. 4e, segment 11 on Table 1) to  $-63.4^\circ$  in the mid anterior (Fig. 4a, segment 7 on Table 1). The transmural profiles of TA using

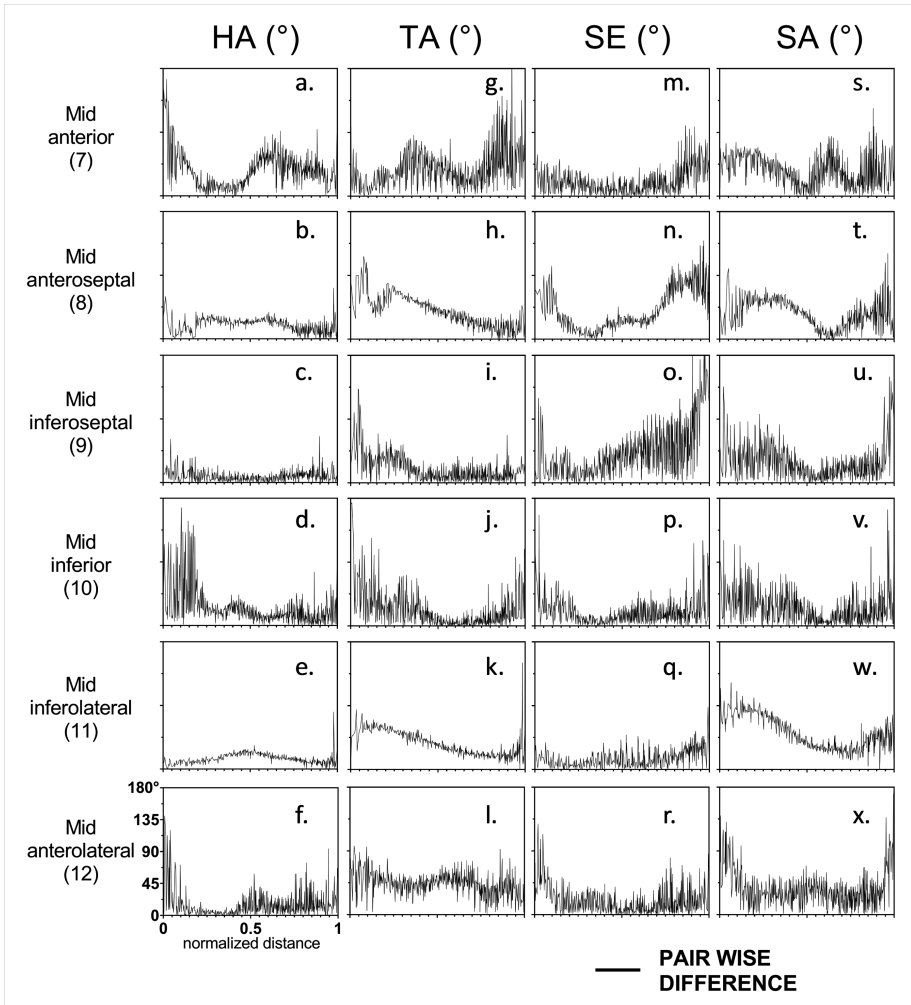


**Fig. 5.** Pair wise difference between DTI and STI in myocytes and sheetlet orientations. The 17-segment AHA model defines regions and AHA7-12 of pair wise difference (black line) of helix angle (HA), transverse angle (TA), sheet elevation (SE) and sheet azimuth (SA) are displayed.

STI (Fig. 4g–l) have a low linearity ( $R^2 \leq 0.34$ ). We can notice that the slope of  $111.7^\circ$  in the mid anteroseptal (Fig. 4b, segment 7 on Table 1),  $97.2^\circ$  in the mid inferoseptal (Fig. 4c, segment 9 on Table 1) and  $-61.5^\circ$  in the mid inferolateral (Fig. 4e, segment 9 on Table 1) appears to be not close to  $0^\circ$ .

**Laminar Orientation.** Quantitative maps of standard angles describing the laminar orientation (SE, SA) for both DTI and STI are presented (Fig. 3e–h). Based on DTI eigenvectors, SE map (Fig. 3e) is heterogeneous in the lateral regions of the LV from the sub-epicardium ( $80\text{--}90^\circ$ ) to the sub-endocardium (close to  $0^\circ$ ) while the septal



region is uniform and close to 0°. In comparison with STI, SE map (Fig. 3f) reveals the same trend as the DTI but with a more moderate elevation (45°). For SA map using DTI (Fig. 3g) we observe homogeneous values, and the angle values are close to 0°. Both SA and SE maps present an abrupt separation between the LV and RV orientation. The STI SA map (Fig. 3h) shows values close to 0° in the sub-epicardium and about -90° in the sub-endocardium. The intersection between the LV and RV are more homogeneous than with DTI SA and SE maps.

Transmural profiles of SE and SA of DTI and STI in the mid ventricular region as measured in segment 7 to 12 based are presented (Fig. 4m-x), their linearity and slope summarized (Table 2) and the pair wise difference between the profiles of DTI and STI is presented (Fig. 5m-x).

The DTI transmural profiles of SE (Fig. 4m-r) are not linear ( $R^2 \leq 0.13$ ) and the slope range is broad with -19.8° in the mid inferior region (Fig. 4p, segment 10 on Table 2) and 73.8° in the mid inferolateral region (Fig. 4q, segment 11 on Table 2). Moreover, the pair wise difference of SE (Fig. 5m-r) shows a globally constant variation between DT and ST in the transmural profile for the segments 7 and 10 to 12 (Fig. 5m and p-r). The pair wise difference of SA (Fig. 5s-x) displays a less consistent variation between STI and DTI for segment 7 and 11 (Fig. 5q and w), which decreases from 70-90° in the sub-endocardium to 10-20° in the middle of the wall and then increases to 30-40° in the sub-epicardium.

In comparison, STI transmural profiles of SE (Fig. 4m-r) have a lower linearity, than DTI ( $0.01 \leq R^2 \leq 0.25$ ) and the slope of 44.1° in the mid inferolateral (Fig. 4q, segment 11 on Table 2) is small in comparison with DTI slope of 73.8° in the same region (Fig. 4q, segment 11 on Table 1). The DTI SA transmural profiles (Fig. 4s-x) displays the non-linearity ( $R^2 \leq 0.22$ ) and a broad slope range even if the septal region (Fig. 4n-o, segment 8-9 on Table 2) is of a greater homogeneity. For STI, Transmural profiles of SA (Fig. 4s-x) have the overall same linearity and slope range as the DTI (Table 2).

**Table 2.** Linearity (R2) and coefficient slope of DTI and STI laminar orientation (sheet elevation angle and sheet azimuth angle). Linearity and slope were measured from LV endocardium to epicardium.

	DTI Sheet elevation		STI Sheet elevation		DTI Sheet azimuth		STI Sheet azimuth	
	Linearity	Slope	Linearity	Slope	Linearity	Slope	Linearity	Slope
	7	0.01	12.2 ± 1.5	0.01	-21.5 ± 3.0	0.16	48.3 ± 1.6	0.12
8	0.10	44.8 ± 1.8	0.23	-95.0 ± 2.4	0.08	40.5 ± 1.9	0.33	-111.9 ± 2.2
9	0.00	-2.6 ± 3.0	0.25	-108.2 ± 2.8	0.1	51.2 ± 2.3	0.09	-58.7 ± 2.8
10	0.02	-19.8 ± 2.0	0.03	-34.1 ± 2.8	0.01	-13.7 ± 1.9	0.02	-26.5 ± 3.0
11	0.13	73.8 ± 2.6	0.09	44.1 ± 1.9	0.02	-21.2 ± 2.0	0.12	46.9 ± 1.7
12	0.06	29.0 ± 1.7	0.05	49.0 ± 2.9	0.22	65.8 ± 1.8	0.00	-2.5 ± 3.5

## 4 Discussion and Conclusion

This study presents a comparison between 3D DTI and STI using a processing pipeline allowing the investigation of cardiac microstructure in the whole human heart. The STI data processed using a FLASH/ST sequence are acquired at an isotropic resolution of  $150 \times 150 \times 150 \mu\text{m}^3$ , and DTI images are obtained on a volume at  $600 \times 600 \times 600 \mu\text{m}^3$ . Both acquisitions are post processed and compared using tensor imaging with an isotropic resolution of  $600 \times 600 \times 600 \mu\text{m}^3$ . Here, we show for the first time full 3D reconstructions of myocardial myocytes and sheetlet orientation in a human heart using Structure Tensor Image Analysis.

Myocyte orientation characterized by STI demonstrated that transmural profiles of HA and TA (Fig. 4a–l) are consistent with a previous study on rodent heart [13].

Cardiac laminar organization is more complex. Indeed, Gilbert et al. [13] and Bernus et al. [14] demonstrated that laminar structure has many regions of localized structural complexity. Thus, that it is not possible to label unique laminae and unequivocally determine their dimensions using one eigenvector since they form a densely branching three-dimensional network with more than one preferred direction and high spatial change of the laminar orientation [5]. The strong non-linearity of SE and SA in both DTI and STI (Table 2) is consistent with the discontinuous nature of myolaminar organization. Nonetheless, we observed strong similarities in 3D on SE and SA maps (Fig. 3e–h) between STI and DTI.

The pair wise difference between DTI and STI transmural profiles (Fig. 5a–x) highlights the consistency of HA and TA calculations in all regions even though there is an offset (more than  $20^\circ$ ) between DTI and STI measurements as demonstrated by Bernus et al. [14]. Laminar organization is more complex and the comparison between SA and SE is more challenging particularly in the septal region (segments 7 to 9), and the junction of the two ventricles. We also need to improve our STI pipeline, especially concerning the angles unwrapping on the edges.

Bernus et al. [14] have shown a bias between DTI and STI (more than  $20^\circ$ ) on rat hearts and emphasized the fact that the assignment of eigenvectors for DTI could provide limited assessment of laminae directions. DTI has an important role for describing myocyte orientation and STI is reliable for myolaminar measurements, we can hypothesize that combining both techniques in one acquisition could lead to the exploitation of the best of each one.

STI pipeline has been developed for rat hearts and applied to a human heart in our study. The first STI at  $150 \times 150 \times 150 \mu\text{m}^3$  allows us to perform a 3D volume giving a large amount of structure information (size of ventricles, vessels, etc.) and the consequence in the case of a human heart is a loss of SNR (SNR = 90 for FLASH/ST at  $150 \times 150 \times 150 \mu\text{m}^3$  against 479 for DTI at  $600 \times 600 \times 600 \mu\text{m}^3$  in the same region). Moreover, some spatial heterogeneities have been observed, which could be reduced by adapting the STI pipeline to large volumes. There are discrepancies in different segments but also similarities. We can identify good similarities between segments. Nevertheless, we identify noisier results on segments 7 and 10, which correspond to the junction between RV and LV cardiac muscle and a specific

organization of tissues in these areas. More investigation in several areas, especially in base apex region, LV/RV junction have to be studied.

In conclusion, these preliminary results are a promising foundation for investigating the 3D structural characterization of normal/pathologic cardiac organization. This work could be useful for simulation especially if we applied the pipeline on pathological heart. It could be integrate to provide information to better understand the inverse problem of electrocardiography, as it will serve to ameliorate the regularization techniques that help solve ill-posed problem

## References

1. Hooks, D.A., Trew, M.L., Caldwell, B.J., Sands, G.B., LeGrice, I.J., Smaill, B.H.: Lamina arrangement of ventricular myocytes influences electrical behavior of the heart. *Circ. Res.* **101**(10), e103–e112 (2007)
2. Streeter Jr., D.D., Spotnitz, H.M., Patel, D.P., Ross Jr., J., Sonnenblick, E.H.: Fiber orientation in the canine left ventricle during diastole and systole. *Circ. Res.* **24**(3), 339–347 (1969)
3. Rohmer, D., Sitek, A., Gullberg, G.T.: Reconstruction and Visualization of Fiber and Sheet Structure with Regularized Tensor Diffusion MRI in the Human Heart, Lawrence Berkeley National Laboratory (2006)
4. Gilbert, S.H., Benson, A.P., Li, P., Holden, A.V.: Regional localization of left ventricular sheet structure: integration with current models of cardiac fiber, sheet and band structure. *Eur. J. Cardiothorac. Surg.* **32**(2), 231–249 (2007)
5. LeGrice, I.J., Smaill, B.H., Chai, L.Z., Edgar, S.G., Gavin, J.B., Hunter, P.J.: Lamina structure of the heart: ventricular myocyte arrangement and connective tissue architecture in the dog. *Am. J. Physiol.* **269**(2 Pt 2), H571–H582 (1995)
6. Toussaint, N., Stoeck, C.T., Schaeffter, T., Kozerke, S., Sermesant, M., Batchelor, P.G.: In vivo human cardiac fiber architecture estimation using shape-based diffusion tensor processing. *Med. Image Anal.* **17**(8), 1243–1255 (2013)
7. Nielles-Vallespin, S., et al.: Assessment of myocardial microstructural dynamics by in vivo diffusion tensor cardiac magnetic resonance. *J. Am. Coll. Cardiol.* **69**(6), 661–676 (2017)
8. Holmes, A.A., Scollan, D.F., Winslow, R.L.: Direct histological validation of diffusion tensor MRI in formaldehyde-fixed myocardium. *Magn. Reson. Med.* **44**(1), 157–161 (2000)
9. Teh, I., et al.: Resolving fine cardiac structures in rats with high-resolution diffusion tensor imaging. *Sci. Rep.* **6**, 30573 (2016)
10. Helm, P.A., Tseng, H.J., Younes, L., McVeigh, E.R., Winslow, R.L.: Ex vivo 3D diffusion tensor imaging and quantification of cardiac lamina structure. *Magn. Reson. Med.* **54**(4), 850–859 (2005)
11. Healy, L.J., Jiang, Y., Hsu, E.W.: Quantitative comparison of myocardial fiber structure between mice, rabbit, and sheep using diffusion tensor cardiovascular magnetic resonance. *J. Cardiovasc. Magn. Reson.* **13**, 74 (2011)
12. Köhler, S., Hiller, K.H., Waller, C., Jakob, P.M., Bauer, W.R., Haase, A.: Visualization of myocardial microstructure using high-resolution  $T_2^*$  imaging at high magnetic field. *Magn. Reson. Med.* **49**(2), 371–375 (2003)
13. Gilbert, S.H., et al.: Visualization and quantification of whole rat heart lamina structure using high-spatial resolution contrast-enhanced MRI. *Am. J. Physiol. Heart Circ. Physiol.* **302**(1), H287–H298 (2012)

14. Bernus, O., et al.: Comparison of diffusion tensor imaging by cardiovascular magnetic resonance and gadolinium-enhanced 3D image intensity approaches to investigation of structural anisotropy in explanted rat hearts. *J. Cardiovasc. Magn. Reson.* **17**, 31 (2015)
15. Sacolick, L.I., Wiesinger, F., Hancu, I., Vogel, M.W.:  $B_1$  mapping by Bloch-Siegert shift. *Magn. Reson. Med.* **63**(5), 1315–1322 (2010)
16. Tustison, N.J., et al.: N4ITK: improved N3 bias correction. *IEEE Trans. Med. Imaging* **29**(6), 1310–1320 (2010)
17. Gilbert, S.H., Smaill, B.H., Walton, R.D., Trew, M.L., Bernus, O.: DT-MRI measurement of myolaminar structure: accuracy and sensitivity to time post-fixation, b-value and number of directions. In: *Conference Proceedings of IEEE Engineering in Medicine and Biology Society*, pp. 699–702 (2013)
18. Gilbert, S., Trew, M., Smaill, B., Radjenovic, A., Bernus, O.: Measurement of myocardial structure: 3D structure tensor analysis of high resolution MRI quantitatively compared to DT-MRI. In: Camara, O., Mansi, T., Pop, M., Rhode, K., Sermesant, M., Young, A. (eds.) *STACOM 2012. LNCS*, vol. 7746, pp. 207–214. Springer, Heidelberg (2013). [https://doi.org/10.1007/978-3-642-36961-2\\_24](https://doi.org/10.1007/978-3-642-36961-2_24)
19. Fedorov, A., et al.: 3D slicer as an image computing platform for the quantitative imaging network. *Magn. Reson. Imaging* **30**(9), 1323–1341 (2012)
20. Cerqueira, M.D., et al.: Standardized myocardial segmentation and nomenclature for tomographic imaging of the heart. A statement for healthcare professionals from the Cardiac Imaging Committee of the Council on Clinical Cardiology of the American Heart Association. *Circulation* **105**, 539–542 (2002)